IEEE Robotics and Automation Letters (RA-L) paper, presented at ICRA 2026, Vienna, Austria. Cite as RA-L paper.

Bi-Stable Thin Soft Robot for in-Plane Locomotion in Narrow Space

Xi Wang, *Member, IEEE*, Yihan Liu, Junhao Tu, Jung-Che Chang, Feiran Wang, Dragos Axinte, and Xin Dong

***Abstract*—Dielectric elastomer actuators (DEAs), also recognised as artificial muscle, have been widely developed for the soft locomotion robot. With the complaint skeleton and miniaturised dimension, they are well suited for the narrow space inspection. In this work, we propose a novel low profile (1.1 mm) and lightweight (1.8 g) bi-stable in-plane DEA (Bi-DEA) constructed by supporting a dielectric elastomer onto a flat bi-stable mechanism. It has an amplified displacement and output force compared with the in-plane DEA (I-DEA) without the bi-stable mechanism. Then, the Bi-DEA is applied to a thin soft robot, using three electrostatic adhesive pads (EA-Pads) as anchoring elements. This robot is capable of crawling and climbing to access millimetre-scale narrow gaps. A theoretical model of the bi-stable mechanism and the DEA are presented. The enhanced performance of the Bi-DEA induced by the mechanism is experimentally validated. EA-Pad provides the adhesion between the actuator and the locomotion substrate, allowing crawling and climbing on various surfaces, i.e., letter and acrylic. The thin soft robot has been demonstrated to be capable of crawling through a 4 mm narrow gap with a speed up to 3.3 mm/s (0.07 body length per second and 2.78 body thickness per second).**

***Index Terms*—Soft robot materials and design, compliant joints and mechanisms, dielectric elastomer actuator (DEA), narrow space locomotion, low profile.**

I. Introduction

NARROW space inspection is commonly seen in human life and industry, especially in scenarios humans cannot access. Robots play a significant role in those fields [1], i.e., continuous robots with small diameters have been developed to access the gas turbine and conduct repair work [2], [3]; A hexapod robot with an embedded machine tool can get into a hazardous environment for maintenance tasks [4]. However, these robots usually have a large volume, complex actuation system, and rigid profile, which will be a limitation in fragile and high-precision scenarios.

Soft robots can overcome those drawbacks with the inherent complaint body, compact profile, lightweight, simple control strategy and reliable human-machine interaction [5]. Many actuation methods have been investigated and applied in locomotion soft robot development. A quadruple pneumatic robot crawled through a 2cm narrow gap using a soft body with a 9mm thickness [6]. The pneumatic chamber with reinforced fiber was capable of controllable deformation [7]. Therefore, an inchworm-inspired soft robot can perform multimodal locomotion of crawling, climbing and transition [8]. Another benefit of the pneumatic actuator is the electronic-free achieved by a buckling-sheet ring oscillator; it also has multimodal movement in various terrains [9]. Most attempts to use the pneumatic robots in narrow space access rely on their complaint body. But, reducing the dimension from centimetre to millimetre scale is a big challenge for pneumatic actuation. Piezoelectric actuated robots have fast responses and more compact volumes. It has been designed into sub-gram with a low profile and can fast-moving 20 body lengths per second [10]. However, it only worked on horizontal locomotion. Alternatively, a microrobot could walk on the vertical and inverted substrate by adding four electrostatic adhesive pads onto a quadrupedal piezoelectric actuated frame [11]. But the dimension still limits its access to millimetre-scale narrow space due to the robot design.

Another actuation option for the soft locomotion robot is the dielectric elastomer actuator (DEA) which is outstanding for its fast response, high energy density and lightweight [12]. Two typical linear DEAs can be applied to soft crawling robots, i. e., cylindrical (spring-roll) linear DEA [13] and saddle-shaped DEA [14], [15]. A pipeline inspection robot consists of a 6mm diameter middle cylindrical DEA as a linear actuator and two shorter DEAs as anchoring feet that can crawl into a pipe [13]. The saddle-shaped DEA worked as a bending actuator and usually used electro-adhesive pads [14] or unidirectional frictions unit [16] to achieve locomotion. A soft wall climbing robot has been demonstrated crawling through a 10mm height narrow gap [14]. With the development of advanced manufacturing technology, multi-layered dielectric elastomers have become a popular topic among researchers. The integrated multi-layers feature can enhance the energy density of the actuator by increasing the output force and reducing the actuation voltage. Based on this improvement, a unimorph multi-layered bending DEA has been

Received 14 September 2024; accepted 4 May 2025. Date of publication 9 May 2025; date of current version 22 May 2025. This article was recommended for publication by Associate Editor J. Liu and Editor X. Liu upon evaluation of the reviewers' comments. The work of Xi Wang was supported by China Scholarship Council. This work was supported in part by Industrial Strategy Challenge Fund delivered by U.K. Research and managed by Engineering and Physical Sciences Research Council Programme under Grant EP/R026084/1 and Grant EP/P031684/1. *(Corresponding author: Xin Dong.)*

Xi Wang, Jung-Che Chang, Feiran Wang, Dragos Axinte, and Xin Dong are with the Faculty of Engineering, University of Nottingham, NG8 1BB Nottingham, U.K. (e-mail: xi.wang1@nottingham.ac.uk; jung-che.chang@nottingham.ac.uk; feiran.wang@nottingham.ac.uk; dragos.axinte@nottingham.ac.uk; xin.dong@nottingham.ac.uk).

Yihan Liu is with the Department of Bioengineering, Imperial College of Science Technology and Medicine, SW7 2AZ London, U.K. (e-mail: yihan.liu123@imperial.ac.uk).

Junhao Tu is with the University of Michigan, Ann Arbor, MI 48109 USA (e-mail: junhaotu@umich.edu).

Digital Object Identifier 10.1109/LRA.2025.3568605

IEEE Robotics and Automation Letters (RA-L) paper, presented at ICRA 2026, Vienna, Austria. Cite as RA-L paper.

designed into a crawling robot [17]. Taking advantage of the amplified vibration of a system in its natural frequency, some researchers proposed soft robotic insects have fast responses and speed actuated at the system's natural frequency [18], [19]. Although the advances in investigating the small dielectric elastomer actuated soft robot, the minimum dimension is still a centimetre-scale, especially regarding the low profile.

An approach to construct millimetre-scale DEA-based soft robots is to utilise the in-plane deformation of DEAs, reducing the space required during actuator morphing. An all-soft, skin-like millimetre-scale structure was proposed with in-plane deformation, capable of locomotion and transportation [20]. However, one limitation was its low velocity of less than 0.12 mm/s (0.001 body lengths per second). In our prior work, we developed a thin DEA-based soft robot utilising a re-entrant structure that enables in-plane linear deformation, achieving a speed of 2.3 mm/s (0.035 body lengths per second) [21]. One factor limiting the speed was the voltage-induced displacement of the actuator. The negative stiffness bi-stable mechanism is a promising method to enhance the displacement output of the DEA. Common approaches include biasing springs [22], [23], silicone domes [24], and magnetic mechanisms [25]. However, most of these designs rely on 3D configurations, which limit the miniaturisation of DEA dimensions. Our other work introduced a 2D negative stiffness mechanism for DEA using a 3D-printed linkage structure, demonstrated the feasibility of developing negative stiffness DEAs with in-plane deformation [26], and the thickness can potentially be reduced to millimetre-scale. These advancements pave the way for developing millimetre-scale thin soft robots with improved speed performance.

This letter presents the design of a novel Bi-stable thin soft robot that can move and access millimetre-scale narrow gaps on horizontal and vertical substrates. The electrostatic adhesive pads (EA-Pads) are used as the anchoring element [14], [27]. Inspired by the out-of-plane cone-shaped DEA tensioned by a biasing mechanism [22], [25], [28], the displacement and the output force of the DEA can be improved by properly balancing the negative stiffness property of the mechanism with the dielectric elastomer. A bi-stable in-plane dielectric elastomer actuator (Bi-DEA) has been presented. It has a thin feature (1.1 mm) and amplified displacement and output force compared with the in-plane dielectric elastomer actuator (I-DEA) without the bi-stable mechanism. The rest of the letter is organized as follows. Section II shows the structure of the robot and the design principle of the Bi-DEA. Section III illustrates the fabrication and characterisation of the Bi-DEA and the EA-Pad. The experimental results of the robot crawling in narrow spaces on both horizontal and vertical surfaces (letter and acrylic material) have been presented in Section IV.

II. Bi-Stable Thin Soft Robot

A. Robot Design

As illustrated in Fig. 1(a), the bi-stable thin soft robot consists of a Bi-DEA (Fig. 1(b)) for linear motion and three EA-Pads (Fig. 1(c)) for anchoring. The front and rear EA-Pads are fixed at the edge of the rectangular frame, while the middle EA-Pad

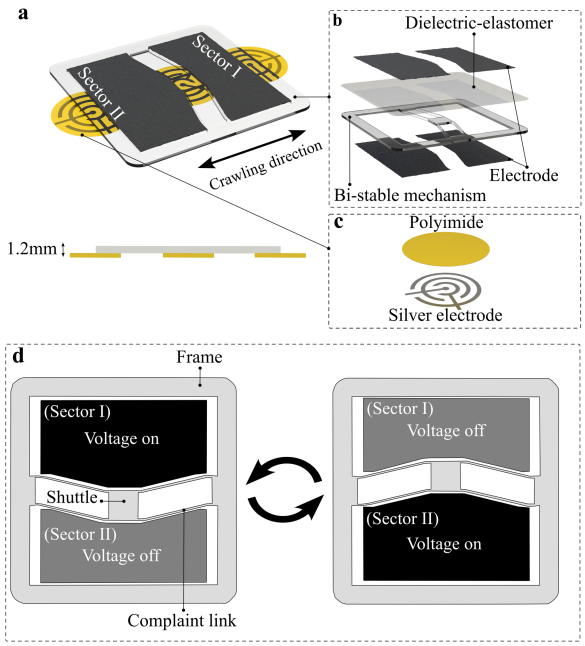

Fig. 1. Concept of Bi-stable thin soft robot. (a) 3D model of Bi-stable thin soft robot; (b) explode view of Bi-DEA; (c) explode view of EA-Pad; (d) actuation principle of Bi-DEA.

is connected with the shuttle of the bi-stable mechanism. 1-DOF (one-degree-of-freedom) crawling locomotion is realized by alternatively charging Sectors I and II of the DEA (Fig. 1(d)). The in-plane motion of the Bi-DEA achieves a thickness of less than 1.2 mm for the robot. Therefore, it can crawl and access narrow spaces.

B. Bi-Stable In-Plane DEA

As illustrated in Fig. 1(b), the novel thin Bi-DEA has a dielectric elastomer sandwiched by electrodes on both sides and further bonded onto a bi-stable mechanism. The bi-stable mechanism consists of a central shuttle connected to a rectangular frame through four complaint links. The shuttle and the complaint links divide the electrode into two sections, i.e., Sectors I and II (Fig. 1(d)). Therefore, the central shuttle can switch between two stable states by applying voltage for Sectors I or II. This bi-stable mechanism with in-plane linear motion can guarantee the thin thickness and improve the voltage-induced displacement and force of the actuator.

An in-plane DEA (I-DEA), as shown in Fig. 2(a), and a bi-stable mechanism (Fig. 2(b)) are proposed to analyze the Bi-DEA displacement and force amplification principle (Fig. 2(c)). The I-DEA and Bi-DEA have the same configuration, except that the I-DEA does not have the bi-stable mechanism (four complaint links). F_D is the force of the I-DEA to the shuttle when the voltage is applied to Sector I. It has seen linear decreases to zero from the point a_1 to a_3 where achieves the maximum displacement ($a_3 - a_1$) of the I-DEA. F_M is the force that moving the shuttle from one stable state a_1 to the another a_5 [29]. For the Bi-DEA in which a bi-stable mechanism is adopted in I-DEA, the output force (shuttle) can be expressed by $F_D - F_M$. The

IEEE Robotics and Automation Letters (RA-L) paper, presented at ICRA 2026, Vienna, Austria. Cite as RA-L paper.

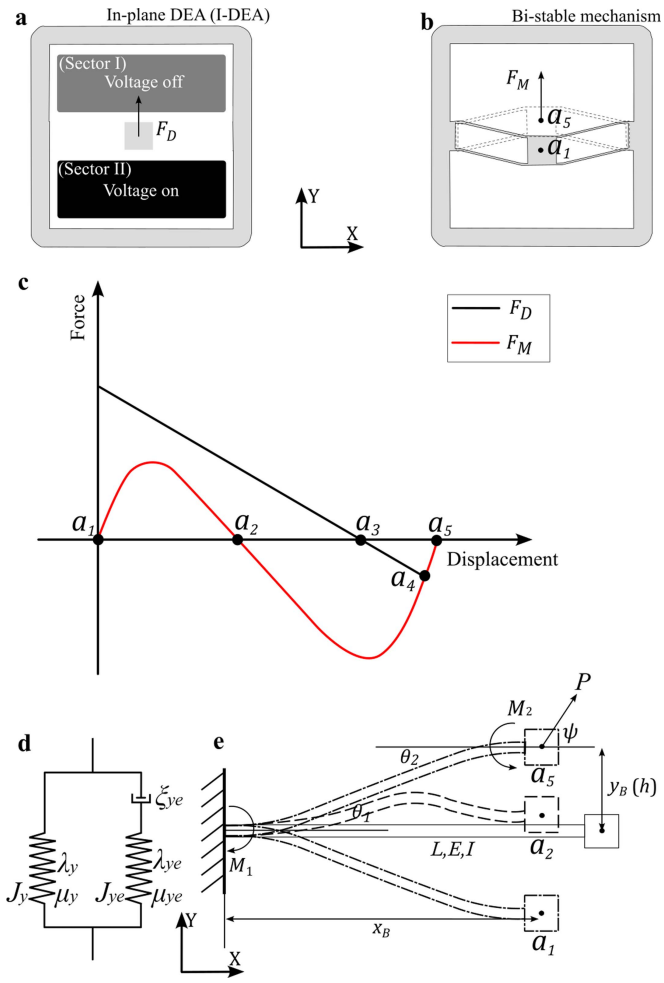

Fig. 2. Principle and analysis of Bi-DEA. (a) I-DEA; (b) Bi-stable mechanism; (c) force-displacement diagram of DEA and bi-stable mechanism; (d) sketch of the elastomer deformation represented by a spring-dashpot system (Bergstrom-Boyce model [26], [31]); (e) sketch of a fixed-guided beam.

maximum displacement is $a_4 - a_1$ at which point the force goes down to zero ($F_D - F_M = 0$). Therefore, the displacement and the output force of Bi-DEA can be larger than the I-DEA if the force of the dielectric elastomer and the mechanism match properly, i.e., $a_4 - a_1 > a_3 - a_1$ and $F_D - F_M > F_D$.

For the I-DEA with the actuated Sector II, as shown in Fig. 2(a), the spring-dashpot system illustrated in Fig. 2(d) is used to model the response in the Y direction. Based on the non-equilibrium thermodynamic theory [30] and using the Bergstrom-Boyce model [31] to characterize the dielectric elastomer, the voltage-induced stress can be expressed as

$$\sigma_y = \mu_{ye}\frac{\lambda_y^2\xi_{ye}^{-2} - \lambda_y^{-2}\lambda_x^{-2}\xi_{ye}^2\xi_{xe}^2}{1 - \frac{\lambda_y^2\xi_{ye}^{-2}+\lambda_x^2\xi_{xe}^{-2}+\lambda_y^{-2}\lambda_x^{-2}\xi_{ye}^2\xi_{xe}^2-3}{J_{ye}}} + \mu_y\frac{\lambda_y^2 - \lambda_y^{-2}\lambda_x^{-2}}{1 - \frac{\lambda_y^2+\lambda_x^2+\lambda_y^{-2}\lambda_x^{-2}-3}{J_y}} - \varepsilon {E_v}^2 \quad (1)$$

where λ_x and λ_y are the strain of the elastomer in X and Y directions, they are calculated through $\lambda_x = \frac{l_x}{L_x}$ and $\lambda_y = \frac{l_y}{L_y}$, ($L_x$ and L_y are the initial length of the elastomer in the X and Y directions while l_x and l_y represent the corresponding length after pre-stretch and actuation). Further, $\lambda_y = \lambda_{ye}\,\xi_{ye}$; μ_y, μ_{ye}, J_y and J_{ye} are shear modulus and stretch limit of elastomer, as shown in the Fig. 2(d); ε is the permittivity of the dielectric elastomer, $E_v = \frac{U}{l_z}$ (U is the input voltage and l_z is the thickness of the elastomer). Therefore, for a cross-section of $l_x \times l_z$ of Sector II, the output force is

$$F_D = l_x\, l_z \sigma_y \quad (2)$$

When the shuttle of the bi-stable mechanism moved from one stable state a_1 to the another a_5, the F_M is comes from the deformation of four complaint links. Each complaint link can be simplified as a fixed-guided beam modelled (Fig. 2(e)) by the elliptic integral solution [32], [33]. The fixed end is connected with the square frame, and the guided end is fixed with the shuttle. The following equations can describe the relation between reaction force and displacement of the guided end [34]:

$$\sqrt{\alpha} = F(k,\phi_2) - F(k,\phi_1) \quad (3)$$

$$\frac{y_B}{L} = -\frac{1}{\sqrt{\alpha}}\{2k\cos\psi(\cos\phi_1 - \cos\phi_2) + \sin\psi \times [2E(k,\phi_2) - 2E(k,\phi_1) - F(k,\phi_2) + F(k,\phi_1)]\} \quad (4)$$

$$\frac{x_B}{L} = -\frac{1}{\sqrt{\alpha}}\{2k\sin\psi(\cos\phi_2 - \cos\phi_1) + \cos\psi \times [2E(k,\phi_2) - 2E(k,\phi_1) - F(k,\phi_2) + F(k,\phi_1)]\} \quad (5)$$

where $\alpha = \frac{PL^2}{EI}$ is the non-dimensional force, $\frac{x_B}{L}$ and $\frac{y_B}{L}$ are the non-dimensional lengths of the guided end of the beam in X and Y directions; L, E and I are the length, Young's modulus and moment of inertia of the beam; P and ψ are the reaction force and the angle with respect to the X axis; $F(k,\phi)$ and $E(k,\phi)$ are incomplete elliptic integrals of the first and second kind; k is the elliptic modulus, ϕ is the amplitude of the elliptic integral and it changes continuously from ϕ_1 at the fixed end (θ_1) to $\emptyset_2$ at the guided end (θ_2). The ϕ also can be calculated by [34]:

$$k\,\sin\phi = \cos\frac{\psi - \theta}{2} \quad (6)$$

$$M_{1,2} = 2k\sqrt{EIP}\cos\phi_{1,2} \quad (7)$$

where M_1 and M_2 are the moment of two ends of the beam, θ is the deformation angle.

As shown in Fig. 2(e), the boundary condition is $\theta_1 = \theta_2 = 0$ in the process of the guided end moves from a_1 to a_5. Therefore, the ϕ can be expressed as follow:

$$\sin\phi_{1,2} = \frac{1}{k}\cos\frac{\psi}{2} \quad (8)$$

For the bi-stable mechanism in this letter, the complaint link has gone through two order modes, therefore, ϕ_1 is the principal solution of (8). For the first order mode, $\phi_2 = \pi - \phi_1$; For the second order mode, $\phi_2 = \phi_1 + 2\pi$.

When the coordinates of the beam's guided end (x_B, y_B) are known, the force and moment at the beam's end (P, M) can be numerically determined. Starting with initial values for ψ and k,

IEEE Robotics and Automation Letters (RA-L) paper, presented at ICRA 2026, Vienna, Austria. Cite as RA-L paper.

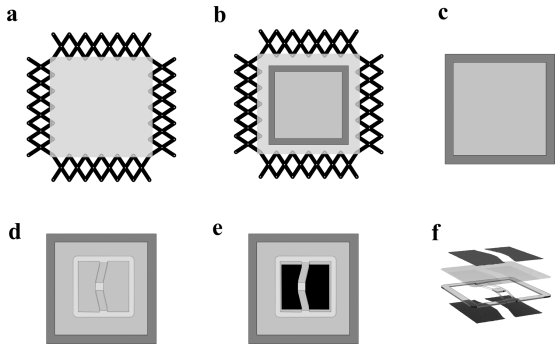

Fig. 3. Fabrication of the Bi-DEA. (a) Pre-stretch the elastomer; (b) adhere an acrylic frame onto the pre-stretched elastomer; (c) transfer the pre-stretched elastomer to the acrylic frame; (d) fix the bi-stable mechanism onto the pre-stretched elastomer; (e) paint electrode; (f) explode view of the Bi-DEA.

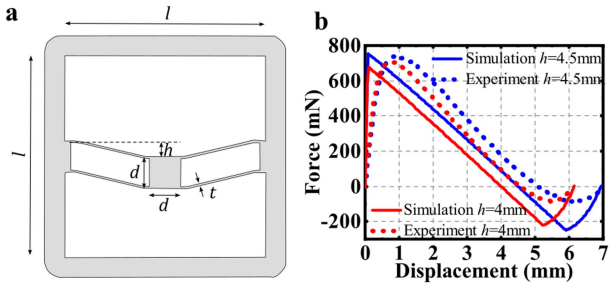

Fig. 4. Characterisation of Bi-stable mechanism. (a) Layout and dimensions of the Bi-stable mechanism; (b) Experimental and simulation diagram of force and displacement of the Bi-stable mechanism.

a numerical iteration process based on (3)–(5) can be applied to refine the values of ψ and k. Then, the load at the guided end can be computed. The reaction force of the shuttle in the Y direction is

$$F_M = 4P \sin\psi \tag{9}$$

III. Fabrication and Characterisation

A. Fabrication

Fig. 3 shows the fabrication process of the Bi-DEA. A 1mm thick dielectric elastomer (3M VHB 4910) was pre-stretched by 4.5∗4.5 times [21] using the fixture in Fig. 3(a). In Fig. 3(b) and (c), the pre-stretched elastomer was transferred to a rigid acrylic frame. Then, a bi-stable mechanism was cut from a 1mm thick PETG sheet using the laser cutter (Jindiao Technology Co., Ltd, JD3050). Its shuttle was then manually switched to second stable state (a_5, as illustrated in Fig. 2(b)) and fixed to the elastomer (Fig. 3(d)). We used multi-walled carbon nanotube as the electrode paints on both sides of the elastomer, as shown in Fig. 3(e). Finally, the Bi-DEA was finished by cutting off the acrylic frame (Fig. 3(f)). Based on this fabrication procedure, the actuator has a 1.1 mm thickness and 1.8 g weight.

The EA-Pad was fabricated by inkjet printing the electrode onto a polyimide film (diameter: 25 mm; thickness: 0.025 mm) to the structure, as illustrated in Fig. 1(c). The silver electrodes were printed using a Fujifilm Dimatix Materials Printer DMP2850 Series and a 2.4 pL Samba cartridge loaded with the XTPL IJ-36 silver nanoparticle ink. The droplet diameter is 40 µm, and a drop spacing of 20 µm was used to ensure the deposition of continuous layers and pattern uniformity. Six layers were printed on a polyimide substrate, and the substrate was heated to 80 °C by an in-situ resistance heater to pin the droplets. The printed samples are then sintered at 150 °C for an hour to enhance electrical conductivity [35]. This manufacturing method could achieve a thin thickness of 0.028mm and a smooth electrode surface with a sheet resistance of 0.24±0.05 Ω/sq in the pad.

B. Characterisation of Bi-DEA

Based on the analysis of the working principle of Bi-DEA, the force of the dielectric elastomer and the bi-stable mechanism should be balanced to achieve one stable state in voltage off status. Applying the voltage to one Sector, the voltage-induced force is generated, resulting in the shuttle being moved to the second stable state. As presented in the fabrication of the Bi-DEA, the pre-stretch ratio of VHB was 4.5∗4.5, which means the force provided by the elastomer is fixed. Therefore, we need to design the parameters of the bi-stable mechanism to fit F_M with F_D, as illustrated in Fig. 2(c).

Calculating the bi-stable mechanism based on the mathematical model, Fig. 4(a) presents the layout and dimension. An 8mm∗8mm inner central shuttle is connected to a 50mm∗50mm square inner frame through four 0.6 mm width flexible links. The central shuttle is biasing from the centre of the frame with a distance of h, designed as a variable to explore how the bi-stable property can be optimised. The experimental setup used for this measurement is shown in Fig. 5(a). A load cell (Omega LCMFD-10N) was installed on a linear motor (Maxon EPOS 2) and further connected to the shuttle through a lightweight beam. During the measurement, the motor dragged the shuttle at a speed of 0.1 mm/s while the load recorded the reaction force. We investigated the force-displacement diagram of the bi-stable mechanism with the h of 4 mm and 4.5 mm, as shown in Fig. 4(b). It was noticed that a larger biasing distance h has a larger displacement and resistant force between two stable states. The error between the simulation and experimental data is attributed to the laser cutting of the compliant link into such a small dimension (0.6 mm), which reduced its stiffness due to the laser cutting process.

We characterised the performance of the Bi-DEA and further compared it with the I-DEA to illustrate how the in-plane bi-stable mechanism help to improve the displacement and the output force of the DEA. Fig. 5(a), (b) presents the experimental setup of the characterisation. The experimental results of the I-DEA and two types of Bi-DEA ($h = 4$ mm and $h = 4.5$ mm) are illustrated in Fig. 6. Applying step signal to Sector II of the DEAs while Sector I remain voltage off, Fig. 6(a) records the displacement of the central shuttle in different voltages. The I-DEA has a larger displacement than the Bi-DEAs when the electric field strength is less than 70 V/um (3.5kV). At 80V/um (4 kV), the displacement of Bi-DEA has dramatically increased to 4.35 mm ($h = 4$ mm) and 6.71 mm ($h = 4.5$ mm) from 2.89 mm (I-DEA), which is an improvement of 151% and 232%, respectively. This is because the bi-stable mechanism has been switched from one stable state to another, which results

IEEE Robotics and Automation Letters (RA-L) paper, presented at ICRA 2026, Vienna, Austria. Cite as RA-L paper.

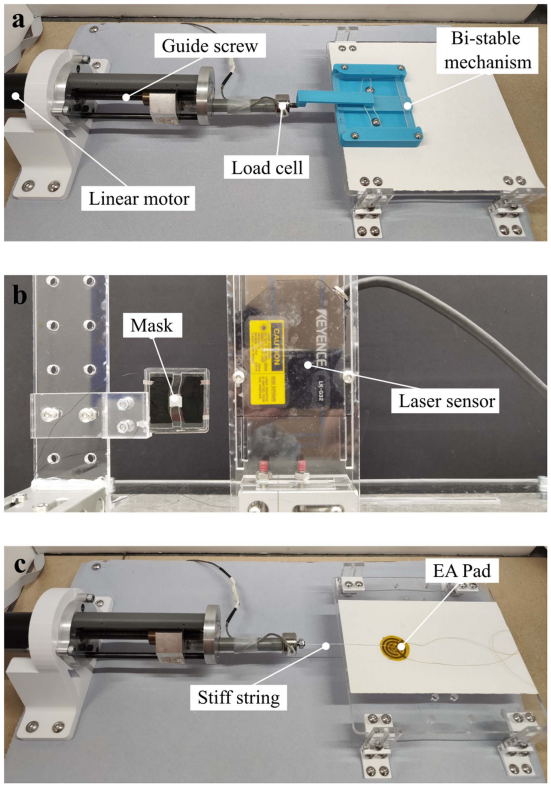

Fig. 5. Experimental setup. (a) Bi-stable mechanism and Bi-DEA force measurement; (b) Bi-DEA displacement measurement; (c) EA pad tangential force measurement.

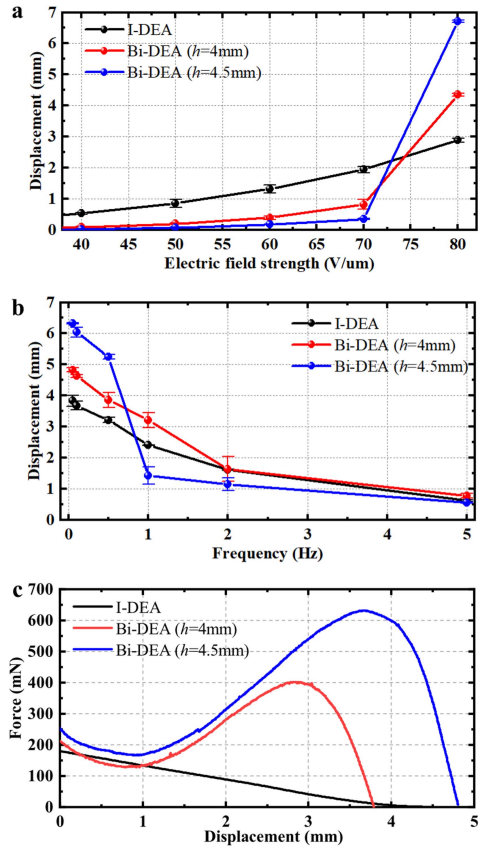

Fig. 6. Characterisation of the Bi-DEA. (a) Diagram of displacement-electric field strength (the error bar is the standard deviation of three measurements); (b) diagram of displacement-frequency (the error bar is the standard deviation of three measurements); (c) diagram of force-displacement.

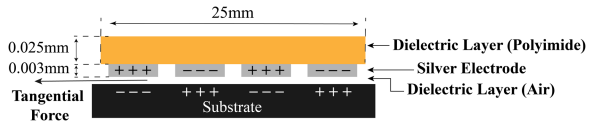

Fig. 7. Working principle of EA-Pad.

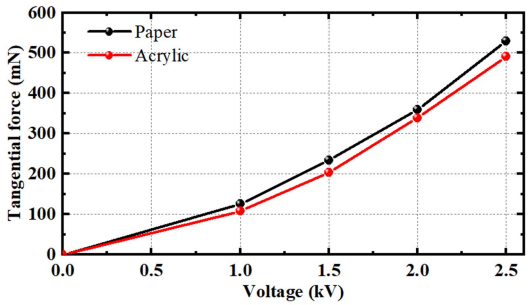

Fig. 8. Tangential force of EA-Pad on letter and acrylic substrate.

in displacement amplification. Fig. 6(b) is the displacement in different frequencies at 80V/um (4kV). The square signal was used to actuate Sectors I and II, resulting in the central shuttle switching between two stable states. The displacement amplitude decreased when the frequency increased for all three DEAs. The Bi-DEA ($h = 4$ mm) has a larger displacement when the frequency rises from 1–2 Hz. Furthermore, the Bi-DEA ($h = 4.5$ mm) has the largest displacement at a lower frequency (0–0.5 Hz). Fig. 6(c) investigates the output force of the DEAs with the displacement increase, in which Sector II was actuated by the step signal (80 V/um, 4kV) and no voltage for Sector I. Three DEAs have a similar force value when the displacement is zero due to the same configuration in the measurement (The shuttle was fixed by the load cell. Therefore, the force at zero displacement is determined by the voltage-induced force of Sector II). The I-DEA shows a linear decrease in force when the displacement increases. In contrast, the force of Bi-DEAs has improved when the displacement is larger than 1mm. The maximum force of Bi-DEA ($h = 4$ mm) is 400 mN, while the Bi-DEA ($h = 4.5$ mm) is 630 mN. This comes from the bi-stable mechanism, at which point ($\sim$1mm displacement) the central shuttle has been pushed to the second stable state, and the force of the mechanism is reversed.

C. Characterisation of EA-Pad

Fig. 7 illustrates the principle of the EA-Pad with a circular interdigitated geometry. A tangential force is generated between the pad and the substrate with voltage applied. The tangential force of the EA-Pad was measured using the equipment shown in Fig. 5(c). During the measurement, the motor dragged the pad moving at a constant speed of 0.1 mm/s on the substrate. Fig. 8 shows the tangential force of the EA-Pad on letter and acrylic substrate. The value was measured by applying a step signal

IEEE Robotics and Automation Letters (RA-L) paper, presented at ICRA 2026, Vienna, Austria. Cite as RA-L paper.

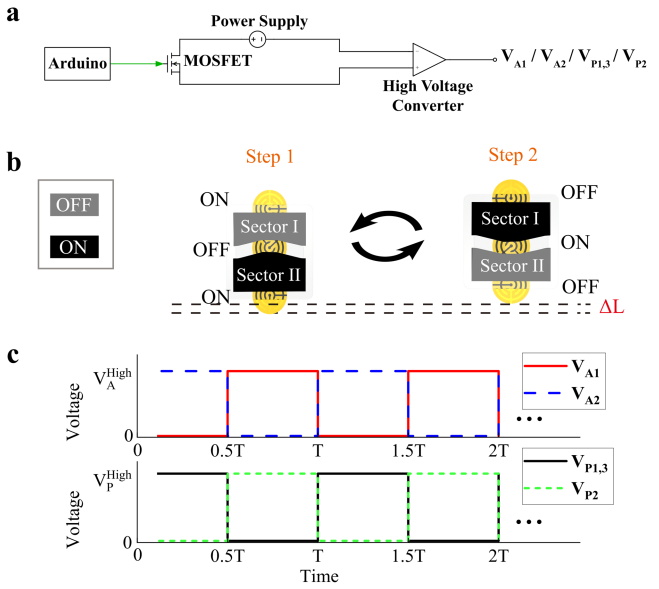

Fig. 9. Control of the bi-stable thin soft robot. (a) Schematic of the control system; (b) locomotion gait; (c) Sequences of controlled voltages.

voltage for the EA-Pad. It can be seen the force increased with the voltage from 0 to 2.5 kV. The maximum tangential force is 490 mN on the acrylic surface and 549 mN on the letter. The differences are caused by the friction coefficient between the pad and acrylic (Ra 2 um) plate is smaller than that of letter (Ra 3 um).

IV. Experiment and Demonstration

A. Gait Design

Fig. 9(a) presents the control system for the Bi-stable thin soft robot, the MOSFETs (IRF540N) connected with a power supply and programmed by the microcontroller (Arduino Mega 2560). It can generate a square signal sequence, further amplified by the high voltage converter (XP-Power Q101-5) to actuate the Bi-DEA and EA-Pads. To achieve stable crawling, a three EA-Pad configuration is adopted. Two EA-Pads, positioned at the front and back of the frame, are actuated simultaneously, while the third EA-Pad is placed on the middle shuttle. This configuration ensures stable and robust adhesion to the wall during climbing. The motion of the Bi-DEA (controlled by V_{A1} and V_{A2}) is synchronized with the adhesion of the EA-pads (controlled by $V_{P1,3}$ and V_{P2}). The crawling of the robot is divided into repeated cycles, T, and each cycle consists of two steps, which is demonstrated in Fig. 9(b) and (c). In the first step (from 0 to 0.5 T), the voltage of the front and rear EA-Pad, $V_{P1,3}$, increased from 0 V to V_P^{High}, which caused these pads to adhere to the substrate. At the same time, the applied voltage for the Sector II of DEA, V_{A2}, rose from 0V to V_A^{High} and that for Sector I, V_{A1}, was at 0 V. In this case, the shuttle and the middle EA-Pad is pushed upward by Sector II. In the second step (from 0.5T to T), the voltage applied to the middle pad increased from 0V to V_P^{High} while the $V_{P1,3}$ drop to 0V. This causes the middle pad to adhere to the substrate but the front and rear pads to release from the substrate. With the V_{A1} and V_{A2} changing to V_A^{High} and 0V, respectively, the shuttle moved downward and pushed the robot forward at a distance ΔL. To achieve a higher crawling speed, the Bi-DEA ($h = 4$ mm) has a higher $\Delta L \times (1/\mathrm{T})$ and will be adopted in Bi-stable thin soft robot.

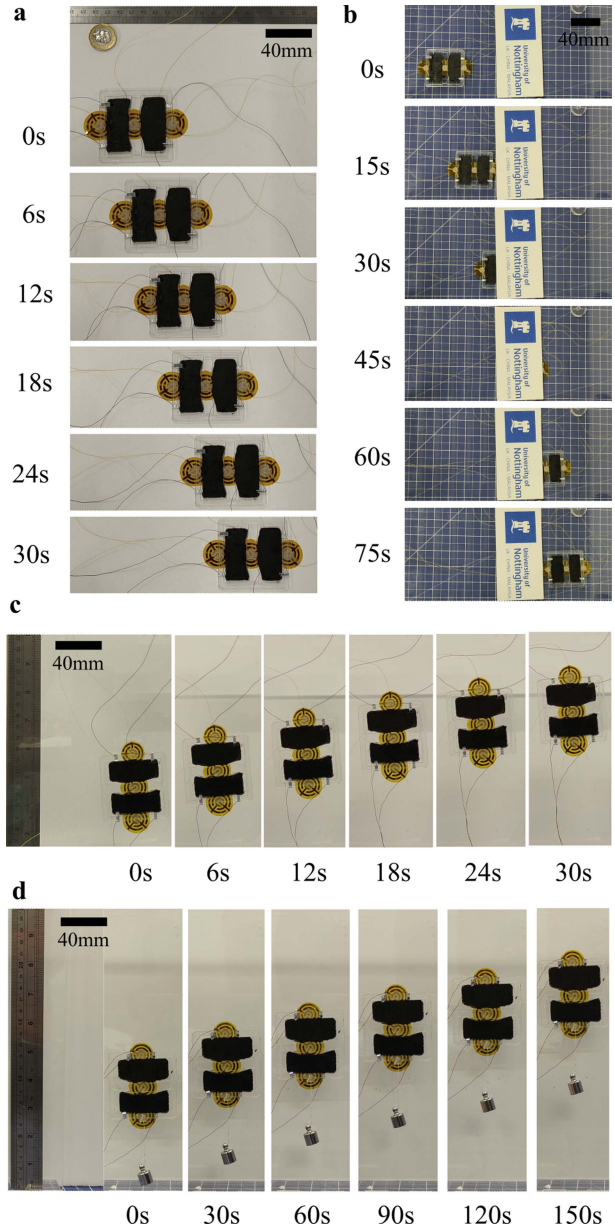

Fig. 10. Locomotion results of the thin soft robot. (a) Horizontal crawling on letter; (b) horizontal crawling and accessing a narrow gap on acrylic plate; (c) vertical climbing on acrylic plate; (d) vertical climbing with a 10g payload on an acrylic plate.

B. Crawling

We demonstrated the robot's ability to crawl on various substrates, using letter and acrylic for the experiments. Fig. 10(a) shows still images of the robot crawling horizontally on a letter substrate over 30 seconds (see Supplemental Video S1). In this

IEEE Robotics and Automation Letters (RA-L) paper, presented at ICRA 2026, Vienna, Austria. Cite as RA-L paper.

TABLE I
COMPARISON OF BI-DEA WITH CURRENT EXISTING DEA WITH NEGATIVE STIFFNESS MECHANISM

Reference	Dimension (length*width*height)	Strain (displacement per body length[1])	Displacement amplification ratio	Dielectric layer material	Displacement per thickness[2]
This work	50*50*1.1	13.4%	232%	VHB 4910	611%
[26]	60*12*65	9.1%	32.7%	Elastosil 2030	50%
[25]	~60*60*80	4.0%	166%	SNES-18602-19RT5	5.3%
[23]	70*70*25	6.4%	160%	Silicone material	6.4%
[38]	30*30*15	14%	-	Elastosil 2030	14%
[39]	20*20*10	46%	-	VHB 4910	46%

Note: [1] The body length is the dimension along the actuated deformation direction; [2] The thickness is calculated the minimum dimension among the length, width and height.

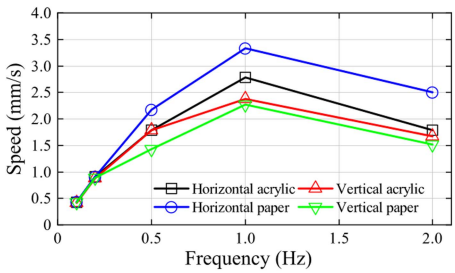

Fig. 11. Locomotion speeds of the bi-stable thin soft robot.

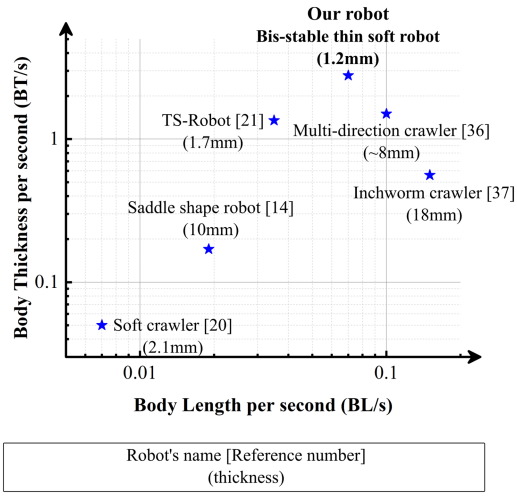

Fig. 12. Performance comparison of our robots with other DEA-based robots with EA-Pad anchoring element. (The speed data for the saddle-shaped robot was calculated based on its crawling demonstration in a confined space with a height of 10 mm, the speed data for the inchworm crawler was calculated based on its crawling demonstration in a confined space with a height of 18 mm).

scenario, the robot achieved a maximum speed of 3.33 mm/s (0.07 body length per second and 2.78 body thickness per second) at a frequency of 1 Hz. As illustrated in Fig. 11, the crawling speed increased with frequency from 0.1 Hz to 1 Hz and slightly decreased at 2 Hz. This trend is consistent with the performance of the Bi-DEA shown in Fig. 6(b). Fig. 10(b) demonstrates the robot successfully navigating a 4 mm narrow gap on the acrylic substrate (see Supplemental Video S2).

C. Vertical Crawling

We further evaluated the robot's vertical climbing performance (see Supplemental Video S3). As shown in Fig. 10(c), the robot achieved a maximum vertical climbing speed of 2.38 mm/s on an acrylic substrate (Fig. 11). The vertical speeds were generally lower than the horizontal speeds, particularly at higher frequencies. This is due to the DEA having to overcome its own weight during vertical climbing, which reduces the displacement in each cycle. Additionally, we investigated the robot's potential for confined space inspection. The Bi-DEA generates an output force of up to 400 mN, while the EA-Pad can provide an adhesion force of up to 549 mN. As demonstrated in Fig. 10(d), the robot's payload capacity was tested by successfully climbing vertically on the acrylic substrate while carrying a constant weight of 10 g, which is five times the robot's own weight.

V. CONCLUSION

In this letter, we presented a bi-stable thin soft robot with a thickness of 1.2 mm, capable of accessing a 4 mm narrow space both horizontally and vertically on various substrates. The robot consists of two sections: a Bi-DEA and three EA-Pads. The Bi-DEA features amplified displacement and output force by employing an in-plane bi-stable mechanism in the I-DEA. This enhancement increases the displacement to 6.71 mm, representing a 232% improvement over the I-DEA, while the maximum output force rises from 180 mN to 630 mN. In addition to the enhanced displacement and force properties, the Bi-DEA maintains a low profile (1.1 mm) and lightweight design (1.8 g), making it ideal for miniaturised thin locomotion robots. Table I highlights the outstanding performance of Bi-DEA with current existing negative stiffness mechanism. The three EA-Pads, which serve as adhesive feet, are integrated with the Bi-DEA. The electrodes of the EA-Pads are directly printed onto a 0.025 mm polyimide sheet, resulting in a total thickness of just 0.028 mm. The tangential force between the pad and substrate reaches 549 mN on letter and 490 mN on acrylic. Thanks to these advantages, we demonstrated the superior performance of the bi-stable thin soft robot compared to the state-of-the-art DEA-based soft robots using EA-Pads [36], [37] as anchoring elements for narrow space access and locomotion (Fig. 12). The robot achieved a maximum speed of 3.33 mm/s, which corresponds to 0.07 body length per second and 2.78 body thickness per second, highlighting its potential for applications in narrow space access and inspection.

ACKNOWLEDGMENT

The authors would like to acknowledge Centre for Additive Manufacturing, University of Nottingham for printing of the EA pad.

IEEE Robotics and Automation Letters (RA-L) paper, presented at ICRA 2026, Vienna, Austria. Cite as RA-L paper.

REFERENCES

[1] D. Axinte, "Portable robotised machines tools (RoboMach), for in-situ inspection and (re)manufacture: Research challenges and opportunities," *Int. J. Mach. Tools Manufacture*, vol. 195, Feb. 2024, Art. no. 104115.

[2] X. Dong et al., "Continuum robots collaborate for safe manipulation of high-temperature flame to enable repairs in challenging environments," *IEEE-ASME Trans. Mechatron.*, vol. 27, no. 5, pp. 4217–4220, Oct. 2022.

[3] W. Ba, X. Dong, A. Mohammad, M. Wang, D. Axinte, and A. Norton, "Design and validation of a novel fuzzy-logic-based static feedback controller for tendon-driven continuum robots," *IEEE-ASME Trans. Mechatron.*, vol. 26, no. 6, pp. 3010–3021, Dec. 2021.

[4] X. Dong, D. Palmer, D. Axinte, and J. Kell, "In-situ repair/maintenance with a continuum robotic machine tool in confined space," *J. Manuf. Processes*, vol. 38, pp. 313–318, 2019.

[5] H. Hussein et al., "Actuation of Mobile microbots: A review," *Adv. Intell. Syst.*, vol. 5, 2023, Art. no. 2300168.

[6] R. F. Shepherd et al., "Multigait soft robot," *Proc. Nat. Acad. Sci. United States Amer.*, vol. 108, no. 51, pp. 20400–20403, Dec. 2011.

[7] N. S. Usevitch, A. M. Okamura, and E. W. Hawkes, "APAM: Antagonistic pneumatic artificial muscle," in *Proc. IEEE Int. Conf. Robot. Automat.*, 2018, pp. 1539–1546.

[8] Y. Zhang, D. Yang, P. Yan, P. Zhou, J. Zou, and G. Y. Gu, "Inchworm inspired multimodal soft robots with crawling, climbing, and transitioning locomotion," *IEEE Trans. Robot.*, vol. 38, no. 3, pp. 1806–1819, Jun. 2022.

[9] W. K. Lee et al., "A buckling-sheet ring oscillator for electronics-free, multimodal locomotion," *Sci. Robot.*, vol. 7, no. 63, Feb. 2022, Art. no. eabg5812.

[10] Y. C. Wu et al., "Insect-scale fast moving and ultrarobust soft robot," *Sci. Robot.*, vol. 4, no. 32, Jul. 2019, Art. no. eaax1594.

[11] S. D. de Rivaz, B. Goldberg, N. Doshi, K. Jayaram, J. Zhou, and R. J. Wood, "Inverted and vertical climbing of a quadrupedal microrobot using electroadhesion," *Sci. Robot.*, vol. 3, no. 25, 2018, Art. no. eaau3038.

[12] G. Y. Gu, J. Zhu, L. M. Zhu, and X. Zhu, "A survey on dielectric elastomer actuators for soft robots," *Bioinspiration Biomimetics*, vol. 12, no. 1, Jan. 2017, Art. no. 011003.

[13] C. Tang et al., "A pipeline inspection robot for navigating tubular environments in the sub-centimeter scale," *Sci. Robot.*, vol. 7, no. 66, 2022, Art. no. eabm8597.

[14] G. Gu, J. Zou, R. Zhao, X. Zhao, and X. Zhu, "Soft wall-climbing robots," *Sci. Robot.*, vol. 3, no. 25, 2018, Art. no. eaat2874.

[15] D. Wang et al., "Dexterous electrical-driven soft robots with reconfigurable chiral-lattice foot design," *Nature Commun.*, vol. 14, no. 1, 2023, Art. no. 5067.

[16] Y. H. Sun et al., "Origami-inspired folding assembly of dielectric elastomers for programmable soft robots," *Microsystems Nanoeng.*, vol. 8, no. 1, pp. 11, Mar. 2022.

[17] M. Duduta, F. Berlinger, R. Nagpal, D. R. Clarke, R. J. Wood, and F. Z. Temel, "Tunable multi-modal locomotion in soft dielectric elastomer robots," *IEEE Robot. Automat. Lett.*, vol. 5, no. 3, pp. 3868–3875, Jul. 2020.

[18] X. Ji et al., "An autonomous untethered fast soft robotic insect driven by low-voltage dielectric elastomer actuators," *Sci. Robot.*, vol. 4, no. 37, 2019, Art. no. eaaz6451.

[19] C. Tang, B. Y. Du, S. W. Jiang, Z. Wang, X. J. Liu, and H. C. Zhao, "A review on high-frequency dielectric elastomer actuators: Materials, dynamics, and applications," *Adv. Intell. Syst.*, vol. 6, 2024, Art. no. 2300047.

[20] J. L. Guo, C. Q. Xiang, A. Conn, and J. Rossiter, "All-soft skin-like structures for robotic locomotion and transportation," *Soft Robot.*, vol. 7, no. 3, pp. 309–320, Jun. 2020.

[21] X. Wang, S. Li, J.-C. Chang, J. Liu, D. Axinte, and X. Dong, "Multimodal locomotion ultra-thin soft robots for exploration of narrow spaces," *Nature Commun.*, vol. 15, no. 1, 2024, Art. no. 6296.

[22] M. Hodgins, A. York, and S. Seelecke, "Modeling and experimental validation of a bi-stable out-of-plane DEAP actuator system," *Smart Mater. Structures*, vol. 20, no. 9, Sep. 2011, Art. no. 094012.

[23] M. Hodgins, A. York, and S. Seelecke, "Experimental comparison of bias elements for out-of-plane DEAP actuator system," *Smart Mater. Structures*, vol. 22, no. 9, Sep. 2013, Art. no. 094016.

[24] S. Croce, J. Neu, J. Hubertus, S. Seelecke, G. Schultes, and G. Rizzello, "Model-based design optimization of soft polymeric domes used as nonlinear biasing systems for dielectric elastomer actuators," *Actuators*, vol. 10, no. 9, pp. 25, Sep. 2021.

[25] P. Loew, G. Rizzello, and S. Seelecke, "A novel biasing mechanism for circular out-of-plane dielectric actuators based on permanent magnets," *Mechatronics*, vol. 56, pp. 48–57, Dec. 2018.

[26] X. Wang, L. Raimondi, D. Axinte, and X. Dong, "Investigation on a class of 2D profile amplified stroke dielectric elastomer actuators," *J. Mechanisms Robot.*, vol. 17, 2025, Art. no. 031008.

[27] H. Wang, A. Yamamoto, and T. Higuchi, "Electrostatic-motor-driven Electroadhesive robot," in *Proc. 25th IEEE/RSJ Int. Conf. Intell. Robots Syst.*, 2012, pp. 914–919.

[28] M. Hodgins and S. Seelecke, "Experimental analysis of biasing elements for dielectric electro-active polymers," *Proc. SPIE*, vol. 7976, pp. 866–879, 2011.

[29] Z. F. Zhou, Y. Z. Gao, L. N. Sun, W. Dong, and Z. J. Du, "A bistable mechanism with linear negative stiffness and large in-plane lateral stillness: Design, modeling and case studies," *Mech. Sci.*, vol. 11, no. 1, pp. 75–89, Mar. 2020.

[30] Z. Suo, "Theory of dielectric elastomers," *Acta Mechanica Solida Sinica*, vol. 23, no. 6, pp. 549–578, 2010.

[31] G.-Y. Gu, U. Gupta, J. Zhu, L.-M. Zhu, and X. Zhu, "Modeling of viscoelastic electromechanical behavior in a soft dielectric elastomer actuator," *IEEE Trans. Robot.*, vol. 33, no. 5, pp. 1263–1271, Oct. 2017.

[32] G. L. Holst, G. H. Teichert, and B. D. Jensen, "Modeling and experiments of buckling modes and deflection of fixed-guided beams in compliant mechanisms," *J. Mech. Des.*, vol. 133, no. 5, pp. 10, May 2011.

[33] F. L. Ma, G. M. Chen, and G. B. Hao, "Determining the range of allowable axial force for the third-order beam constraint model," *Mech. Sci.*, vol. 9, no. 1, pp. 71–79, Feb. 2018.

[34] L. L. Howell, "Compliant mechanisms," in *Proc. NSF Workshop*, 2013, pp. 189–216.

[35] G. F. Trindade et al., "Residual polymer stabiliser causes anisotropic electrical conductivity during inkjet printing of metal nanoparticles," *Commun. Mater.*, vol. 2, no. 1, pp. 47, 2021.

[36] K. M. Digumarti, C. J. Cao, J. L. Guo, A. T. Conn, and J. Rossiter, and Ieee, "Multi-directional crawling robot with soft actuators and electroadhesive grippers," in *Proc. IEEE Int. Conf. Soft Robot.*, 2018, pp. 303–308.

[37] T. T. Hu, X. J. Lu, and J. Liu, "Inchworm-like soft robot with multimodal locomotion using an acrylic stick-constrained dielectric elastomer actuator," *Adv. Intell. Syst.*, vol. 5, no. 2, Feb. 2023, Art. no. 2200209.

[38] J. Neu, J. Hubertus, S. Croce, G. Schultes, S. Seelecke, and G. Rizzello, "Fully polymeric domes as high-stroke biasing system for soft dielectric elastomer actuators," *Front. Robot. AI*, vol. 8, Jun. 2021, Art. no. 695918.

[39] M. Follador, M. Cianchetti, and B. Mazzolai, "Design of a compact bistable mechanism based on dielectric elastomer actuators," *Meccanica*, vol. 50, pp. 2741–2749, 2015.